BULLETIN of Cherkasy State Technological University

Journal homepage: https://bulletin-chstu.com.ua/en

Vol. 31 No. 2. 2026

UDC 004.932.2:004.056

DOI: 10.62660/bcstu/2.2026.11

ISSN: 2306-4412

E-ISSN: 2708-6070

Method for detecting the results of digital image cloning in post-processing

Svitlana Hryhorenko*

PhD in Technical Sciences
National University "Odesa Polytechnic"
65044, 1 Shevchenko Ave., Odesa, Ukraine
https://orcid.org/0009-0006-4551-8243

Oleksandr Yevseiev

Senior Lecturer
National University "Odesa Polytechnic"
65044, 1 Shevchenko Ave., Odesa, Ukraine
https://orcid.org/0009-0009-3100-2643

Mykola Voronov

Postgraduate Student
National University "Odesa Polytechnic"
65044, 1 Shevchenko Ave., Odesa, Ukraine
https://orcid.org/0009-0003-2816-0495

Abstract. The relevance of this study is driven by the increasing number of digital image falsification cases and the widespread use of fragment cloning as a common manipulation technique, which poses serious challenges to information security. The aim of this research was to develop and experimentally validate a robust method for detecting digital image cloning under post-processing conditions based on the analysis of the minimum mean block difference matrix, enabling reliable identification and spatial localisation of cloned regions and their original prototypes. The proposed method was based on iterative interval bisection combined with binary cross-analysis of block differences and was implemented in the Matlab environment. The experimental framework included modelling additive Gaussian, multiplicative and impulse noise, JPEG compression, spatial filtering, and combined distortions. Visual fidelity was quantitatively evaluated using the peak signal-to-noise ratio with a threshold value of signal-to-noise ratio PSNR > 37 dB. Computational experiments were conducted on central regions of digital images with a resolution of 512 × 512 pixels. Cloned regions occupied less than 0.85% of the image area, typically ranging from 0.098% to 0.39%, while smaller cloned areas below 0.098% were also considered. The analysis was performed on a randomly selected single colour channel using block-based processing. In the absence of post-processing distortions, the global minimum of the minimum mean block difference function reached zero, resulting in maximum detection performance with a true positive rate of 100%. False positive rate evaluation on original images yielded values of 11%, 7.5%, and 3% for block sizes of 16, 24, and 32, respectively. Although the proposed approach demonstrates high detection sensitivity, the results indicate limitations in suppressing false positives compared to some state-of-the-art methods, highlighting the need for further optimisation

Keywords: peak signal-to-noise ratio; "salt and pepper"; gaussian noise; multiplicative noise; "intersection"; Matlab

Article's History: Received: 11.12.2025; Revised: 20.03.2026; Accepted: 18.05.2026; Published: 26.06.2026

Suggested Citation:
Hryhorenko, S., Yevseiev, O., & Voronov, M., (2026). Method for detecting the results of digital image cloning in post-processing. *Bulletin of Cherkasy State Technological University*, 31(2), 11-26. doi: 10.62660/bcstu/2.2026.11.

*Corresponding author (s.m.hryhorenko@op.edu.ua)

INTRODUCTION

The rapid development of digital technologies and the widespread use of digital images (DI) in the media, social networks, electronic document management systems, digital forensics and information security are leading to an increase in the risks associated with the falsification of visual information. One of the most common and, at the same time, most difficult methods of forgery to detect automatically is the cloning of fragments of digital images, which allows objects to be hidden or duplicated without the use of external image sources. The task of detecting the results of cloning becomes particularly difficult in the context of post-processing of digital images, which almost always accompanies the process of creating or distributing images. Noise overlay, filtering, lossy compression, changing storage formats, and other disruptive influences significantly complicate the detection of cloning traces, as they mask the characteristic features of forgery and reduce the similarity between the corresponding fragments of the clone and its prototype. In real-world scenarios of falsification, such influences are not an exception but a typical practice that requires the development of specialised analysis methods that are resistant to post-processing.

Thus, in the work of G. Gani & F. Qadir (2020), a block-oriented approach was proposed in which discrete cosine transform (DCT) is used to form compact frequency features that are less sensitive to noise, JPEG artefacts, and blurring. Additionally, the use of cellular automata allows for the effective grouping of similar blocks and reduces the number of false positives after post-processing, which ensures increased stability of the matching procedure in combined attacks. A.U. Shehin & D. Sankar (2024) used DCT features together with eigenvalues to form an invariant representation of blocks that preserves discriminatory properties after JPEG compression and blur filtering. The proposed scheme also provides robustness to rotations, allowing stable localisation of forged areas under conditions of complex post-processing and geometric transformations. P. Duszejko *et al.* (2025) the scientific literature and research findings, focusing on techniques that detect image manipulations and localise areas of tampering, utilising both statistical properties of images and embedded hidden watermarks. Passive methods, based on analysing the image itself, are versatile and can be applied across a broad range of cases; however, their effectiveness depends on the complexity of the modifications and the characteristics of the image. Active methods, which involve embedding additional information into the image, offer precise detection and localisation of changes but require complete control over creating and distributing visual materials. Both approaches have their applications depending on the context and available resources.

The work F. Li *et al.* (2022). recommends using Graph Neural Networks, Convolutional Neural Networks, Visual Geometry Group Network with 16 Layers, MobileNet, and Residual Network with 50 Layers. Method uniquely integrates these architectures to effectively detect and analyse multiple types of image forgeries, including image splicing and copy-move forgeries. A. Akram *et al.* (2025) argued that the growing reliance on digital image processing technologies is partly explained by the widespread availability of reliable and efficient image capture technologies. The ease with which image content can be altered using modern image editing technologies creates new challenges for forensic analysis. A structured hybrid system for searching for important objects in images is presented.

Despite the existence of a significant number of approaches to detecting cloning in digital images, most of them demonstrate limited effectiveness in the case of combined disruptive influences or require significant computational resources, complex parameter tuning, or prior training on large data sets. In this context, it is relevant to develop a method for detecting the results of DI cloning in post-processing conditions that combines mathematical soundness, algorithmic transparency, and practical applicability for use in expert and automated analysis systems. The purpose of the article was to develop and experimentally substantiate a method for detecting DI cloning results in post-processing conditions, which is based on the analysis of the minimum block difference matrix and allows for the stable detection and localisation of a clone and its prototype in the presence of noise, lossy compression, and other interfering influences.

MATERIALS AND METHODS

In order to make an informed choice of disturbance parameters that ensure the reliability of the visual perception of digital images, a computational experiment was conducted in the Matlab environment. Computational studies were performed using licensed Matlab software (Kadam *et al.*, 2022; Ghai *et al.*, 2024). The Matlab platform was selected due to its extensive set of built-in functions for image processing, numerical computation, and data visualisation, which enables the implementation of complex experimental pipelines and ensures the reproducibility of results.

For simplicity of presentation, without limiting the generality of the considerations, monochrome DI are considered at this stage of the study. Any DI is the result of discretisation of the domain $D \subset R^2$ and quantisation of the function values $f(x, y)$, $(x, y) \in D$, resulting in $n \times m$ – matrix F with elements $f_{ij} \in \{0,1,\dots, 255\}$, $i = \overline{1, n}$, $J = \overline{1, m}$ and the geometric representation can be a three-dimensional surface S, which is the graph of the function $g(x, y)$, approximating $f(x, y)$ on a multiplicity D of vicoristan elements F, in particular $g(x, y)$ can act as an interpolation spline for elements F, which is assumed below. It is shown $g(x, y)$ that if is a 1[st] degree interpolation spline, then the task of its construction is insensitive to changes in the input data – the brightness values of the pixels of the image. The defined parameter characterising the surface S and, as a result DI, the matrix F as a whole, and at the same time insensitive to small changes in the characteristics of the surface (DI) – V the volume of a cylindrical body T with a generatrix parallel to the axis of the applicator OZ, limited by the surface S and the coordinate plane of the characteristics of differences: $V = \iint g(x, y)\, dxdy$, $g(x, y)$ – 1st degree interpolation spline for elements F.

If $K \subset D$, $P \subset D$ – areas corresponding to areas of the clone/prototype (CP), then they can be matched: $V_k = \iint g(x, y)\, dxdy$, $V_p = \iint g(x, y)\, dxdy$. If the central point was not post-processed, then: $V_k = V_p$, otherwise, due to the insensitivity of the volume calculation problem: $V_k \approx V_p$.

For numerical calculation of volume values using double integrals as a composite quadrature formula, the integral sum for a double integral is used, corresponding to the division of the integration region $L \subset D$, for which the partial region is a square, in the centre of which there is a point with the coordinates of the corresponding pixel. Taking into account that the coordinates of adjacent pixels differ by one unit, it can be assumed that the length of the side of each resulting square, and therefore its area S_{ij}, is equal to 1.

$$\iint_L g(x,y)\,dxdy = \sum_{(i,j)\in L} g(i,j) S_{ij} = \sum_{(i,j)\in L} g(i,j) = \sum_{(i,j)\in L} f_{ij}. \quad (1)$$

For (1), the degree of the interpolation spline does not matter , which eliminates the need to consider a spline of degree higher than one for interpolating the elements of the matrix F in the course of the proposed solution of the problem considered in the work.

Thus, for areas of the CP without subsequent processing of the DI, the following relationship must be satisfied, for which insensitivity to disturbances in the input data is established:

$$\sum_{(i,j)\in P} f_{ij} = \sum_{(i,j)\in K} f_{ij}. \quad (2)$$

And under conditions of additional disruptive actions (DA):

$$\sum_{(i,j)\in K} f_{ij} \approx \sum_{(i,j)\in P} f_{ij}. \quad (3)$$

It is assumed that post-processing after cloning applies to the entire DI. Taking into account the results of the literature review, a block-oriented approach is used for the developed method as the most accurate among the existing ones. It is further assumed that the areas of the CP regions are such that the prototype has at least one $q \times q$ – block that does not belong to the CP intersection area.

Taking into account the experiment, during which the presence $q = 4$, $q = 8$ and $q \geq 16$ the absence of blocks in the original DI $q \times q$ – block for which condition (2) was satisfied were established, the criterion for the presence DI of CP regions in the CP in the absence of additional DA was obtained, according to which, $B^{(P)}$ and $B^{(K)}$ – $q \times q$ – blocks of the CP matrix F DI for which $q \geq 16$ and $B^{(P)} \cap B^{(K)} = \emptyset$, then in order for $B^{(P)}$, $B^{(K)}$ to be corresponding blocks from the CP display in digital images, it is necessary and sufficient to fulfil (2).

Taking into account the obtained criterion, in order to reduce the possibility of false alarms when using the developed method for detecting CP in the control system, the $q \times q$ – blocks for which are further used $q \geq 16$. Taking into account the results of the experiment and the criterion obtained, at this stage of the study, it is assumed that if post-processing of the DI after cloning took place, then the areas of the CP that were identical before it will change less relative to each other than those that differed from the CP and therefore differed from each other before post-processing.

The work quantitatively determines the characteristic of 'block differences' taking into account (3), i.e., taking into account the introduced characteristic of the volume of the corresponding body. Let B_j, $i = \overline{1, n-q+1}$, $j = \overline{1, m-q+1}$, – $q \times q$ –block of the $n \times m$ – matrix of the central system F, for f_{ij} which the element is located at position (1,1). Let us call this type of block B_{ij} the main. Each block B_{ij} is assigned $(n - q + 1) \times (m - q + 1)$ matrix of block differences $M^{(ij)}$ (MBD) with elements $m^{(i,j)}\ k, l$ defined as:

$$m^{(i,j)}_{k,l} = \sum_{t,p=1}^{q} r_{tp}, \quad k = \overline{1, n-q+1}, \; l = \overline{1, m-q+1}, \quad (4)$$

where r_{tp}, $t, p = 1, q$ – elements of the $q \times q$ –matrix R, which is obtained as follows:

$$R = \left| B_{ij} - B_{kl} \right|, \quad (5)$$

where equality (5) is understood in an element-by-element sense. The elements of MBD $M^{(ij)}$ reflect the difference between block B_{ij} and any other block of the matrix DI in the sense of (4)-(5), and therefore determine those blocks that differ least from B_{ij} (in terms of the volumes of the corresponding cylindrical bodies), without intersecting with it, and are sought, given the task under consideration.

The established differences $M^{(ij)}$ in properties in B_{ij} cases where belongs/does not belong to the CP region. $\min M^{(ij)} = m^{(i,j)} = 0$. Small in comparison with other elements $M^{(ij)}$ will also be $m^{(i,j)}{}_k$, $k \in \{i - 1, i, i + 1\}$, $l \in \{j - 1, j, j + 1\}$. However, the smallness of these elements is not an indicator of the similarity of the blocks corresponding to them in the sense considered in the work. Therefore, for the convenience of further research, the element $m^{(i,j)}{}_{ij}$ of the matrix $M^{(ij)}$ and its 8 closest neighbours are made equal to a number that is large compared to other elements $M^{(ij)}$. The new matrix is denoted $\overline{M}^{(ij)}$ and is called the modified matrix of block differences (MMBD). The minimum element $\overline{M}^{(ij)}$ corresponds to the block B_{kl} of the clone (prototype) if is the B_{ij} – block of the prototype (clone). In this case:

$$\min \overline{M}^{(ij)} = \min \overline{M}^{(kl)}. \quad (6)$$

If is B_{ij} not a CP block, then $min\,\overline{M}^{(ij)}$ in general is not related to $min\,\overline{M}^{(kl)}$ for any arbitrary block B_{kl} that does not intersect B_{ij}.

Taking into account (6), the matrix F DI is matched $(n - q + 1) \times (m - q + 1)$ with the matrix G – the matrix of minimum block differences (MBD), whose element g_{ij}, $i = \overline{1, n-q+1}$, $j = \overline{1, m-q+1}$, reflects the smallest difference in the sense of (4)-(5) of $q \times q$ –block B_{ij} from any other block of the matrix F:

$$g_{ij} = min\,\overline{M}^{(ij)}, i = \overline{1, n-q+1}, j = \overline{1, m-q+1}. \quad (7)$$

The corresponding blocks B_{ij} and B_{kl} CP in G will correspond to coinciding values of global (or local in conditions of significant DA, as shown below) minima:

$$g_{ij} = g_{kl}, \quad (8)$$

where g_{tp} is a global minimum if G, and $g_{tp} = \min\limits_{1 \le i \le n-q+1, 1 \le j \le m-q+1} g_{ij}$ a local minimum if G in there exists such $U(g_{tp})$ for g_{tp} a neighbourhood for that: $\forall g_{ij}, \in (g_{tp})$, $g_{ij} \neq g_{tp}$: $g_{ij} > g_{tp}$. The $U(g_{tp})$ neighbourhood r' of radius is created by elements $g_{t+k, p+l}$, $k, l \in (-r', \ldots, 0, \ldots, r')$.

Thus, the formal parameter found is a convergence index, quantitatively identical for the corresponding blocks of the CP of the DI, including under conditions of additional DA: the value of the global (local) minimum for the MMBD corresponding to the analysed DI. As a quantitative metric for assessing the reliability of perception of the obtained digital images, similar to the approaches widely used in modern scientific publications on digital image processing, computer vision, and information security, the peak signal-to-noise ratio (PSNR) was used in this study. This metric was chosen because of its versatility, ease of calculation, and ability to quantitatively reflect the level of image distortion resulting from the application of disturbing influences (Ali *et al.*, 2022; Hosny *et al.*, 2023). The PSNR metric is based on a comparison of the original (reference) digital image and the processed image and allows the root mean square error between corresponding pixels to be estimated (Khalil *et al.*, 2023). High PSNR values indicate insignificant distortions and preservation of visual quality, whereas a decrease in this indicator corresponds to an increase in noise intensity or information loss. This property makes PSNR a convenient tool for analysing the impact of various disturbing factors, including additive noise, filtering operations, compression artefacts, and other types of signal degradation, on the reliability of visual perception. Moreover, PSNR is a standardised and widely recognised metric that is frequently applied for benchmarking image processing algorithms within a unified evaluation framework. Its use ensures experimental reproducibility and facilitates direct comparison of the obtained results with data reported in related studies. In the context of clone detection in digital images, PSNR is particularly relevant, as it enables the determination of acceptable disturbance thresholds under which visual distortions remain imperceptible to the human observer but may significantly affect the performance of automated detection algorithms. Therefore, the application of PSNR provides a balanced compromise between computational efficiency, interpretability, and practical relevance in the domain of digital forensics and information security.

The PSNR value was calculated according to the generally accepted analytical expression and allowed to quantitatively assess the level of image distortion after the application of disturbing influences and to determine the acceptable limits of parameters under which the visual authenticity of the DI is preserved:

$$PSNR = 10 \cdot lg\left(255^2 \Big/ \left(\frac{1}{mn}\sum_{i,j}\left(f_{ij} - \overline{f}_{ij}\right)^2\right)\right), \quad (9)$$

where f_{ij}, $i = 1, n$, $j = 1, m$ – elements of the matrix of the modified digital image (it is assumed that the reliability of the digital image is preserved if PSNR > 37 dB).

During the experimental procedure, a set of reference digital images was subjected to controlled disturbing influences with varying intensity levels. For each disturbance scenario, the PSNR value was calculated in order to quantitatively evaluate the degree of image degradation. The obtained PSNR values were subsequently analysed to identify threshold intervals corresponding to visually imperceptible distortions and critical degradation levels that significantly affect both human perception and automated clone detection performance. To ensure statistical reliability, each experiment was repeated multiple times with different disturbance parameters and initial image samples. The resulting measurements were averaged to minimise the influence of random fluctuations and noise. Additionally, graphical visualisation of PSNR trends was performed to facilitate comparative analysis and interpretation of the experimental results.

Thus, the proposed methodological framework combines quantitative image quality assessment with systematic parameter variation, enabling a comprehensive evaluation of the impact of disturbing influences on digital image perception and clone detection robustness. The proposed methodology for clone detection is based on an iterative interval bisection strategy combined with binary image analysis and geometric object comparison. The main objective of the method is to localise characteristic extrema in the interpolated matrix G and to identify repeated structural patterns that indicate the presence of cloning in a digital image. At the initial stage, the full analysis interval $[a, b] = [T_{min}, T_{max}]$ was divided into two equal sub-intervals. For each sub-interval, a corresponding cross-section of the interpolated surface is generated. These cross-sections are represented as binary digital images, where pixel values falling within the specified intensity range are assigned logical values, allowing spatial structures to be isolated.

Each binary cross-section is then analysed using standard connected-component and contour detection techniques. The algorithm searches for objects that are identical in shape and size and bounded by closed contours. The presence of such objects is used as a criterion for updating the counters k_1 and k_2, which indicate whether characteristic patterns are detected in the lower or upper sub-interval, respectively. If both cross-sections contain identical objects ($k_1 = k_2 = 1$), the algorithm selects the interval associated with smaller geometric object dimensions, as this region typically corresponds to a more precise localisation of cloning artefacts. The selected interval is then further divided in half, and the procedure is repeated. This iterative refinement continues until the detected objects become point-like, meaning that their area is equal to one pixel. At this stage, the spatial localisation accuracy reaches its maximum resolution, and the iteration process is terminated. The occurrence of point objects in both analysed sub-intervals is interpreted as a reliable indicator of cloning presence in the digital image.

Finally, the coordinates of the detected point objects are extracted, enabling precise localisation of both the cloned region and its original prototype. This spatial correspondence provides direct geometric evidence of duplication and allows verification of the detected falsification. The proposed approach ensured robust detection performance under additional disturbing influences, such as noise and compression artefacts, by progressively narrowing the analysis interval and isolating stable structural features. As demonstrated in the experimental results, the method provides high localisation accuracy while maintaining computational efficiency.

RESULTS AND DISCUSSION

When modelling attacks on DI at this stage of research, various types of disturbing influences are used, in particular Gaussian, multiplicative and Poisson Noise, salt-and-pepper noise, lossy compression, as well as filtering using various spatial and frequency filters. These types of distortions are typical for simulating image post-processing after cloning operations and correspond to approaches that are widely used in modern scientific research in this and related fields (Hamza, 2022; Jain, 2024). It is important to note that the "author" of a falsified image is usually interested in ensuring that the result of the forgery does not attract additional attention from the expert during visual analysis. In this regard, post-processing of a cloned image is carried out taking into account the requirements for preserving its visual authenticity. Given the widespread use of lossy compression formats for storing and transmitting digital images, the modified image is highly likely to be saved in this format. The most common format in practical application is Joint Photographic Experts Group (JPEG), which justifies its use as the basis for modelling attacks. The results of additional perturbations should not normally lead to noticeable visual artefacts in the final DI. This necessitates careful selection of noise, filtering and compression parameters that ensure the reliability of image perception after their application. At the same time, in practice, there may be situations where post-processing of a DI leads to a partial deterioration in its visual quality.

Note that the reliability of visual perception of a DI under such disturbing influence is considered to be preserved, although the subjective assessment of image quality by individual observers may differ. When modelling attacks on digital images at this stage of research, the following types of distortions are used as the most common and practically significant: additive Gaussian Noise, Multiplicative Noise, "Salt And Pepper", lossy compression, and filtering using various types of filters (9). To evaluate the influence of different noise models on the reliability of digital image perception, a series of controlled experiments was performed using additive and impulse noise disturbances with varying intensity parameters. The average PSNR values obtained for the experimental image set under Gaussian, multiplicative, Poisson, and salt-and-pepper noise conditions are presented in Table 1. The values that satisfy the visual authenticity criterion (PSNR > 37 dB) are highlighted in bold.

Table 1. Average PSNR values obtained as a result of applying noise disturbances to digital images from the experimental array

Gaussian Noise with zero mathematical expectation				**Multiplicative Noise**				**"Salt And Pepper"**	
D = 0.0001	D = 0.0005	D = 0.001	D = 0.005	D = 0.0005	D = 0.001	D = 0.005	D = 0.01	D = 0.02	D = 0.001
43.8	**39.1**	34.5	28.3	**42.8**	**40.4**	33.2	30.9	26.2	**39.0**

Source: created by the authors

The results presented in Table 1 demonstrate that low-intensity noise disturbances have a limited impact on perceived image quality, whereas increasing noise density leads to a rapid degradation of visual fidelity. In particular, Gaussian noise with variance values up to D = 0.0005 preserves acceptable perceptual quality, while higher variance levels result in PSNR values below the reliability threshold. A similar trend is observed for multiplicative and impulse noise, where increasing disturbance intensity significantly reduces PSNR. These findings indicate that the robustness of visual perception is highly sensitive to noise magnitude and that only a limited range of disturbance parameters can be considered acceptable for preserving digital image authenticity. In order to analyse the effect of lossy compression on the reliability of digital image perception, additional experiments were conducted using the JPEG format with different quality factor (QF) values. The corresponding average PSNR values obtained for both Tagged Image File Format (TIFF) and JPEG output formats are summarised in Table 2. The results provide quantitative insight into the relationship between compression level and visual distortion.

Table 2. Average PSNR values as a result of resaving a digital image in a lossy format (Jpeg) with different values of the QF

Output format DI	**QF**							
	95	**85**	**75**	**65**	**55**	**45**	**35**	**25**
Tif	**49.0**	**46.8**	**45.4**	**44.0**	**43.4**	**42.6**	**41.5**	**39.0**
Jpeg	**50**	**41.6**	**40.3**	36.4	35.5	35.1	34.4	34.1

Source: created by the authors

As shown in Table 2, decreasing the quality factor leads to a gradual reduction in PSNR values, indicating an increase in compression-induced distortions. For high QF values (above 75), the PSNR remains well above the perceptual reliability threshold, ensuring visually acceptable image quality. However, when the quality factor drops below 55, a noticeable degradation occurs, and PSNR approaches the critical boundary of visual authenticity. These results confirm that aggressive lossy compression significantly affects the reliability of digital image perception and may compromise the effectiveness of subsequent image analysis and forensic procedures. To assess the impact of spatial filtering operations on digital image quality, experiments were performed using averaging, Gaussian, and median filters with different kernel sizes. The corresponding average PSNR values obtained after filtering are presented in Table 3. This analysis allows the evaluation of smoothing effects on image fidelity and perceptual reliability.

Table 3. Average PSNR values as a result of filtering a digital image

Averaging filter of size $p \times p$			**Gaussian filter of size $p \times p$ ($sig = 0.5$)**			Median filter 3×3
$p = 3$	$p = 5$	$p = 7$	$p = 3$	$p = 5$	$p = 7$	
37	32	23	**44**	**44**	**44**	**38**

Source: created by the authors

The data presented in Table 3 indicate that filter type and kernel size play a critical role in determining the level of image distortion. Averaging filters with increasing window size lead to a substantial decrease in PSNR due to excessive smoothing and loss of fine structural details. In contrast, Gaussian filtering with moderate kernel sizes demonstrates higher PSNR stability, preserving visual quality more effectively. The median filter exhibits intermediate performance, reducing impulse noise while maintaining acceptable perceptual fidelity. These results confirm that inappropriate filtering parameters may significantly degrade visual authenticity, whereas carefully selected configurations can preserve reliable image perception. In further modelling of disturbing influences on digital images, "Salt And Pepper" noise will not be used. This is due to the fact that even with acceptable PSNR values (Table 1), the superimposition of such noise leads to the appearance of clearly visible visual artefacts on the disturbed image. In addition, the specificity of this type of noise – the presence of separately located point distortions – does not provide reliable masking of cloning results at low values of the noise intensity parameter *d*. Accordingly, from a practical point of view, this type of disturbance is highly unlikely to be used by the "Author" of DI falsification. A similar conclusion regarding the presence of noticeable visual artefacts can be made for Poisson noise, which is confirmed by the results of visual analysis showing superimposition without localisation of point objects (Fig. 1).

Based on this, at this stage of the study, the following types of transformations were selected as disturbing influences on digital images: Gaussian Noise with zero mathematical expectation and dispersion $D \le 0.0005$ ($D \in \{0.0005;\ 0.0001\}$); Multiplicative Noise with variance $D \le 0.001$ ($D \in \{0.0005;\ 0.001\}$); lossy compression with an arbitrary quality factor QF in the range from 25 to 95 filtering, except for an averaging filter with a mask size $p \ge 5$. Regarding the disruptive effect associated with lossy compression of digital images, it should be noted that although for quality factor values $QF < 65$, the PSNR index for images in JPEG format decreases and becomes less than 37 dB, no visually noticeable artefacts are observed. Given that compression is the most common type of post-processing of DI and does not usually attract the attention of experts, compression options with $QF < 65$ are not excluded from further consideration at this stage of the study, despite the formal decrease in quantitative quality indicators. To study the complex of disturbing influences on DI after cloning, noise with the parameters defined above was superimposed, followed by lossy compression of the images. The compression quality coefficients QF ∈ {65, 75, 85, 95} were selected, since these parameters are the most common and probable from the point of view of practical use during the storage and transmission of DI.

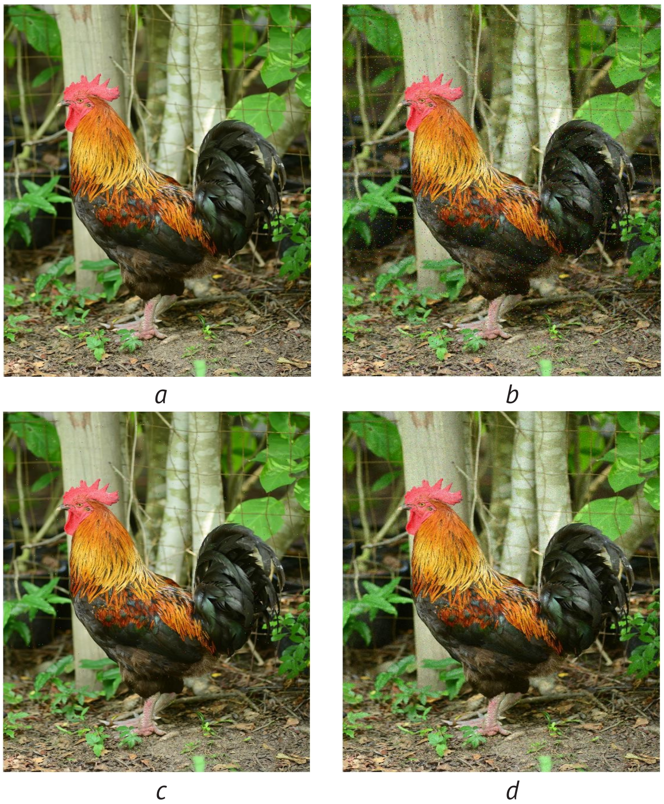

Figure 1. Results of noise superimposition on the DI

Notes: *a* – original DI; *b* – DI after superimposition of "Salt And Pepper" noise with *d* = 0.02; c – "Salt And Pepper" noise with *d* = 0.001; *d* – Poisson Noise

Source: created by the authors

To investigate the combined impact of multiple disturbing factors on digital image quality, an additional series of experiments was performed in which noise disturbances were applied first, followed by lossy JPEG compression with different quality factor values. The resulting PSNR values obtained under complex disturbance conditions are presented in Table 4. This analysis allows the evaluation of cumulative degradation effects and their influence on the reliability of visual perception.

Table 4. PSNR values (dB) after applying complex disturbing effects to a digital image

Output format DI	Gaussian Noise								Multiplicative Noise							
	D = 0.0001				D = 0.0005				D = 0.0005				D = 0.001			
	Subsequent saving in Jpeg with a quality factor QF								Subsequent saving in Jpeg with a quality factor QF							
	QF = 95	QF = 85	QF = 75	QF = 65	QF = 95	QF = 85	QF = 75	QF = 65	QF = 95	QF = 85	QF = 75	QF = 65	QF = 95	QF = 85	QF = 75	QF = 65
Tif	**43.6**	**42.3**	**41.9**	**41.1**	**39.0**	**38.8**	36.9	36.5	**42.7**	**42.5**	**42.3**	**40.0**	**40.3**	**40.0**	**39.5**	**38.7**
Jpeg	**43.7**	**38.9**	**37.2**	36.3	36.9	36.7	36.6	36.2	**41.9**	**38.5**	**37.0**	36.1	**38.7**	**37.5**	36.7	36.0

Source: created by the authors

The results presented in Table 4 demonstrate that the combined application of noise and lossy compression produces a significantly stronger degradation effect compared to the influence of individual disturbances. Even for relatively low noise variance values, subsequent JPEG compression leads to a noticeable reduction in PSNR, indicating cumulative distortion accumulation. In the case of Gaussian noise, high quality factor values (QF = 95 and QF = 85) still maintain PSNR values above the perceptual reliability threshold, whereas further reduction of the quality factor results in values approaching or falling below the critical boundary. A similar trend is observed for multiplicative noise, where increasing noise intensity combined with compression substantially reduces visual fidelity. Furthermore, the comparison between TIFF and JPEG output formats shows that uncompressed or lossless storage formats demonstrate higher robustness against cumulative distortions, while JPEG images exhibit greater sensitivity to compound disturbing effects. This confirms that the sequence of image processing operations and the choice of output format play a crucial role in preserving visual authenticity.

Overall, the obtained results indicate that complex disturbing effects significantly narrow the acceptable parameter range required to maintain reliable digital image perception. These findings are particularly important for digital forensics applications, where multiple processing stages are often applied sequentially and may collectively compromise both visual integrity and the performance of automated detection algorithms. Taking into account the results of subjective quality ranking obtained in the process of applying a complex of disturbing influences to DI, as well as considering the practically reliable fact of storing DIs in lossyy compression formats, even in cases where the PSNR value is less than 37 dB, within the scope of this study, it is considered appropriate to consider the analysed sets of additional disturbing influences (Table 4) as realistically possible scenarios when creating falsified images by cloning.

For the further development of a method for detecting cloning results under the influence of additional disturbing factors, it is important to have information on the quantitative indicators of the difference between the corresponding blocks of the clone and its prototype after post-processing of the DI. In order to determine these indicators, a computational experiment was carried out using digital images from the experimental array. During the experiment, digital images were cloned, with the cloned area and the corresponding original area being square blocks of size $q \times q$, where $q \in \{32, 24, 16\}$. After cloning, Gaussian or Multiplicative Noise was applied to the images with parameters determined in the previous stages of the study as ensuring the reliability of the visual perception of the DI. Next, the images were saved in lossyless (TIF) and lossy (JPEG) formats with different quality coefficients $QF \in \{65, 75, 85\}$. For the images obtained in this way, taking into account that the clone block was denoted as $B^k = B_{ij}$, and the corresponding prototype block as $B^P = B_{kl}$, matrices $\bar{M}^{(ij)}$ and $\bar{M}^{(kl)}$ were constructed. For each pair of such matrices, the minimum values of the selected difference measure were determined, as well as the coordinates of their location. This made it possible to quantitatively assess the degree of similarity between the clone and prototype blocks after applying disturbing influences and post-processing. The results of the computational experiment are presented in Table 5, in which the following designations are used: I – the average value of the indicator for all DI of the experimental array $\min^{(ij)} = \min^{(kl)}$; II and III – the minimum and maximum values of the indicator among all DI involved in the experiment, respectively $\min^{(ij)} = \min^{(kl)}$.

Table 5. Quantitative estimates of the difference between the clone and prototype blocks in terms of (1) – (2) under image post-processing conditions

Block size	Noise type	Noise parameters	Output format DI after cloning		I	II	III
32 × 32	Gaussian noise	D = 0.0001	Tif		2930	2208	3104
			Jpeg	QF = 85	4068	2183	5764
				QF = 75	4357	2113	6764
				QF = 65	4680	1900	7375
		D = 0.0005	Tif		6544	4561	7138
			Jpeg	QF = 85	7242	4429	8592
				QF = 75	6656	4177	9458
				QF = 65	6799	3900	10147
	Multiplicative noise	D = 0.0005	Tif		2650	408	6258
			Jpeg	QF = 85	3930	1169	6231
				QF = 75	4240	1142	7661
				QF = 65	4572	1252	7603
		D = 0.001	Tif		3742	707	7770
			Jpeg	QF = 85	4796	1240	7536
				QF = 75	4941	1370	8572
				QF = 65	5207	1446	8807

Continued Table 5.

Block size	Noise type	Noise parameters	Output format DI after cloning		I	II	III
24 × 24	Gaussian noise	D = 0.0001	Tif		1649	1277	1753
			Jpeg	QF = 85	2325	1181	3670
				QF = 75	2549	1094	4307
				QF = 65	2746	1068	4369
		D = 0.0005	Tif		3687	2593	3994
			Jpeg	QF = 85	4071	2661	4970
				QF = 75	3946	2400	5467
				QF = 65	3889	2080	5940
	Multiplicative noise	D = 0.0005	Tif		1472	309	4917
			Jpeg	QF = 85	2245	701	3470
				QF = 75	2368	634	4261
				QF = 65	2597	711	4290
		D = 0.001	Tif		1967	501	4209
			Jpeg	QF = 85	2564	711	4095
				QF = 75	2671	731	4511
				QF = 65	2690	801	4712
16 × 16	Gaussian noise	D = 0.0001	Tif		911	501	1123
			Jpeg	QF = 85	1007	546	1241
				QF = 75	1111	678	1535
				QF = 65	1247	654	1987
		D = 0.0005	Tif		1698	901	2145
			Jpeg	QF = 85	1814	959	2297
				QF = 75	1746	811	2611
				QF = 65	1800	875	2849
	Multiplicative noise	D = 0.0005	Tif		662	60	1360
			Jpeg	QF = 85	1068	322	1717
				QF = 75	1229	344	1981
				QF = 65	1338	355	2467
		D = 0.001	Tif		1043	235	2290
			Jpeg	QF = 85	1376	401	2211
				QF = 75	1398	484	2268
				QF = 65	1478	489	2329

Source: created by the authors

Based on the data presented in Table 5, the threshold values $T_{min}^{(q)}$ and $T_{max}^{(q)}$ were determined, corresponding, respectively, to the minimum and maximum levels of difference between a clone block of size $q \times q$ and the corresponding prototype block. When solving the problem of finding areas (blocks) of a digital image with minimal differences between each other, each block B_{ij} is assigned a block difference matrix of size $(n-q+1) \times (m-q+1)$, which is further referred to as MAMBD. The elements of this matrix m^{ij}_{kl} are defined as a measure of the difference between block B_{ij} and all other blocks B_{kl} of the analysed digital image:

$$m^{ij}{}_{kl} = \sum_{t,p}^{g} r_{tp},\ k = \overline{1, n-q+1},\ l = \overline{1, m-q+1}, \quad (10)$$

where r_{tp}, $t, p = \overline{1, q}$, are elements of the $q \times q$ matrix R, obtained as follows:

$$R = |B_{ij} - B_{kl}|. \quad (11)$$

In this case, relation (11) is interpreted in an element-by-element sense, i.e., comparison operations are performed for the corresponding pixels of the blocks, which allows for a correct assessment of their similarity after cloning and possible disturbing influences. The obtained threshold values were determined for three levels of the parameter q. In particular, when q equals 32, the minimum threshold value $T_{min}(32)$ is 408, while the corresponding maximum threshold value $T_{max}(32)$ reaches 10,147. For the case where q equals 24, the minimum threshold $T_{min}(24)$ is 309 and the maximum threshold $T_{max}(24)$ is 5,940. Finally, when q equals 16, the minimum threshold $T_{min}(16)$ is equal to 60, whereas the maximum threshold $T_{max}(16)$ amounts to 2,849. These threshold values quantitatively characterise the range of possible differences between the corresponding blocks of the clone and the prototype after cloning and subsequent post-processing of the DI. In addition, it is possible to determine similar threshold values separately for each type of disturbing influence, which is consistent with the approaches presented in S. Grygorenko (2016). In order to formalise the process of detecting cloning results in DI and ensure the possibility of their quantitative analysis, it is advisable to move from the direct analysis of pixel values to the study of specially constructed mathematical objects. This approach allows us to generalise information about local similarities between image fragments, reduce the influence of random noise distortions, and increase the method's resistance to additional disturbing influences. In this context, a key step is to construct an auxiliary matrix that accumulates information about the degree of difference between all possible blocks of a fixed-size DI. Analysis of the properties of this matrix and the nature of its extreme creates a theoretical basis for identifying clone regions and the corresponding prototype, as well as for localising cloning results in the image space.

The main object of analysis during the detection of clone and prototype regions in a DI is the introduction of an $n \times m$ matrix G of size $(n - q + 1) \times (m - q + 1)$ with elements g_{ij}, where $i = \overline{1, n - q + 1}$, $j = \overline{1, m - q + 1}$. The values of the elements g_{i_j} are determined according to the relation: $g_{ij} = \min^{(ij)}$, $i = \overline{1, n - q + 1}$, $j = \overline{1, m - q + 1}$. For this matrix, it is justified that the blocks B_{i_j} and B_{kl}, which correspond to the clone and its prototype, will correspond to the same global (or local) minima in the matrix G, $g_{i_j} = g_{kl}$, which for most DI is an indicator of the presence of cloning and allows its spatial location to be determined. At the same time, in practice, the ratio $g_{i_j} = g_{kl}$ may indicate not the clone and prototype regions, but the original, but slightly different image fragments. In such cases, there is a risk of false cloning identification.

In order to refine the localisation of the clone and prototype areas, it is proposed to use the construction of a set of "sections" of the surface, which is a graph of a function that interpolates the elements of the matrix G. Such "sections" are defined as inequalities $c_1 \leq z \leq c_2$, where c_1, $c_2 = \text{const}$, $c_1, c_2 \in N$, and N is the set of natural numbers. As a result of performing the specified "sections", the coordinates of those blocks of the DI are determined for which the minimum difference from all other blocks in terms of criteria (10) – (11) falls within the specified interval $[c_1, c_2]$. This approach allows for more accurate localisation of potential cloning areas and reduces the number of false positives in the algorithm.

The "sections" is performed according to a specially developed method, which will hereinafter be referred to as the method of dividing the segment in half for the analysis of the matrix of minimum block differences (MAMBD). The proposed method is based on the idea of iterative narrowing of the range of values of the elements of the minimum block difference matrix in order to localise areas that potentially correspond to cloning results. This approach allows for the effective separation of the clone area and its prototype from other structurally similar but original fragments of the DI (Li *et al.*, 2022; Jaiswal *et al.*, 2022). The MAMBD method is an integral part of the basic method of detecting cloning results in DI presented below and performs the function of a refinement stage of analysis. Its application is aimed at increasing the stability of detection against additional disturbing influences, such as noise, filtering and lossy compression, as well as reducing the number of false positives. By using a split-half interval procedure, the method provides adaptive selection of threshold values corresponding to the most informative areas of the surface that interpolates the elements of the minimum block difference matrix (Koul *et al.*, 2022). The main stages of the MAMBD method, outlined below, form a sequential analysis procedure that covers the selection of block representation parameters, the determination of difference thresholds, and the construction of corresponding "sections" for localising potential cloning areas. Together, this creates a methodological basis for the further algorithmic implementation of the method for detecting cloning of DI in post-processing conditions and under the influence of disturbing factors.

Taking into account the specifics of the analysed DI of size $n \times m$ or the geometric parameters of the area "suspicious" from the point of view of cloning, select the size of the analysed block $q \times q$. Then, for the DI, construct a matrix G of size $(n - q + 1) \times (m - q + 1)$, which corresponds to the MAMBD. Determine the threshold values Tmin and Tmax for the possible values of the elements of the matrix G that satisfy the relation $g_{ij} = g_{kl}$, i.e., correspond to the blocks of the clone and its prototype. Hereafter, the element gtp is considered to be the global minimum of the matrix G if it corresponds to the smallest value among all elements within the analysed region. The element gtp is defined as a local minimum if there exists a neighbourhood $U(g_{tp})$ in the matrix G such that, for any element $g_{ij} \in U(g_{tp})$, where $g_{ij} \neq g_{tp}$, the inequality $g_{ij} > g_{tp}$ holds. The neighbourhood $U(g_{tp})$ with radius r is formed by the elements $gt + k, p + l$, where k, $l \in \{-r, \ldots, 0, \ldots, r\}$ k, which enables the analysis of the local region surrounding the considered element.

Given a fixed and uniquely specified block size $q \times q$, the threshold values are taken as $T_{min} = T_{min}^{(q)}$ and $T_{max} = T_{max}^{(q)}$. In the case when additional disturbing influences applied to the DI after cloning are known, the threshold values T_{min} and T_{max} are determined based on the experimental data given in Table 5. If information about the nature of the disturbing influences is missing and the block size q cannot be determined unambiguously, it is advisable to use universal estimates as threshold values to ensure the robustness of the method to uncertainty in the analysis conditions: $T_{min} = \underset{g}{min}\, T_{min}^{(q)}$, $T_{max} = \underset{g}{min}\, T_{max}^{(q)}$. Procedure for dividing the segment in half. At this stage, an iterative division of the analysis interval is performed in order to refine the parameter range and localise characteristic objects in the digital image. First, the initial bounds of the analysis interval are defined: the lower bound $a = T_{min}$ and the upper bound $b = T_{max}$. Then, the midpoint of the interval is calculated as $c = (a + b) / 2$. After determining the midpoint, two cross-sections of the surface representing the graph of the function interpolating the elements of matrix G are generated. The first cross-section corresponds to the interval $a \le z \le ca$, while the second corresponds to $c \le z \le b$. The obtained cross-sections are represented as binary digital images, where white pixels indicate those elements of matrix *G* whose values fall within the corresponding intervals.

Next, the counters $k_1 = 0$ and $k_2 = 0$ are initialised and used to record the presence of characteristic objects in the respective cross-sections. The generated binary images are then analysed using standard digital image processing techniques to detect objects bounded by closed contours. If objects of identical shape and size are detected in the cross-section $a \le z \le c$, the counter k_1 is incremented by one. If, in addition, the area of such objects equals one, meaning that the objects are point-like and isolated, the algorithm proceeds to the next step.

A similar procedure is applied to the cross-section $c \le z \le b$. If objects with identical shape and size are detected, the counter k_2 is incremented. If the area of these objects is equal to one, the algorithm also proceeds to the next step. In the case where $k_1 = 1$ and $k_2 = 0$, the cross-section $a \le z \le c$ is selected for further analysis. The upper bound of the interval is updated as $b = c$, after which a new midpoint is calculated and the procedure returns to the next iteration. If the condition $k_1 = 0$ and $k_2 = 1$ is satisfied, the cross-section $c \le z \le b$ is selected for further analysis. In this case, the lower bound is updated as $a = c$, the new midpoint is calculated, and the next iteration is performed. When $k_1 = k_2 = 1$, the cross-section containing objects with smaller geometric dimensions is selected. If the interval $a \le z \le c$ is chosen, the upper bound is set to $b = c$; otherwise, the lower bound is set to $a = c$. Subsequently, a new midpoint is calculated and the procedure continues. If $k_1 = k_2 = 0$ and, at the same time, the condition $c - a > P$ is satisfied, where P is a threshold value determined experimentally, both cross-sections are subjected to further analysis. For each of them, new interval bounds are defined separately, after which the bisection procedure is repeated. Thus, the interval bisection procedure ensures a gradual narrowing of the search region and increases the accuracy of localising characteristic structures in the digital image, which is a necessary condition for the effective implementation of subsequent stages of the algorithm.

If the condition $k_1 = k_2 = 0$ is true for each of the constructed cuts, then it is concluded that the analysed DI has not been cloned. If $k_1 = 1$ or $k_2 = 1$, it is considered that the analysed DI has been cloned. In this case, the corresponding blocks of the clone and its prototype, which are characterised by the minimum difference between each other in terms of criteria (10) – (11), are determined by isolated identical white objects with an area of 1 (one pixel) on the last binary image slice in order. As methods for processing DI, standard approaches to contour extraction can be applied, in particular the methods proposed and implemented in R. Kundu (2022), Lumenci (2024). For example, gradient methods using the color grading function can be used. During experimental studies using DI from the experimental array, it was found that the threshold value of parameter *P* is 300. To illustrate the proposed method, consider a DI that has been cloned and then subjected to Gaussian Noise with zero mathematical expectation and variance D = 0.0001, and saved in JPEG format with a quality factor QF = 75 (Fig. 2, b).

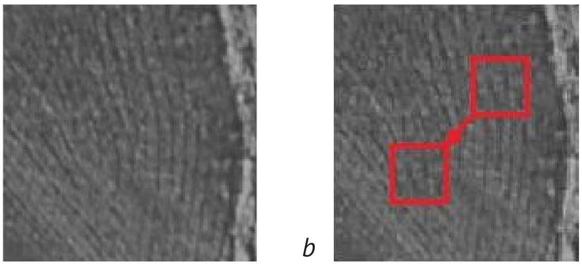

a *b*

Figure 2. DI used to illustrate the operation of MAMBD under conditions of additional disturbing influences
Notes: *a* – original DI; *b* – DI resulting from cloning under conditions of additional disturbing influences
Source: created by the authors

For comparison, the corresponding original DI is shown (Fig. 2). It should be noted that the image under study was deliberately chosen without clearly defined objects, which in general complicates the task of detecting cloning and emphasises the robustness of the proposed approach in conditions of low image structure. First consider a falsified DI (Fig. 2). For its analysis, will use medium-sized blocks with the parameter $q = 24$. According to the data in Table 5, for the selected block size, have the following threshold values: $T_{min} = 1{,}094$, $T_{max} = 4{,} 307$. Figure 3 shows "cross-sections" in the form of binary images obtained as a result of the first division of the segment $[a, b] = [T_{min}, T_{max}]$ in half. Analysis shows that both sections contain objects of the same shape and size within their boundaries, bounded by closed curves, and therefore $k_1 = k_2 = 1$.

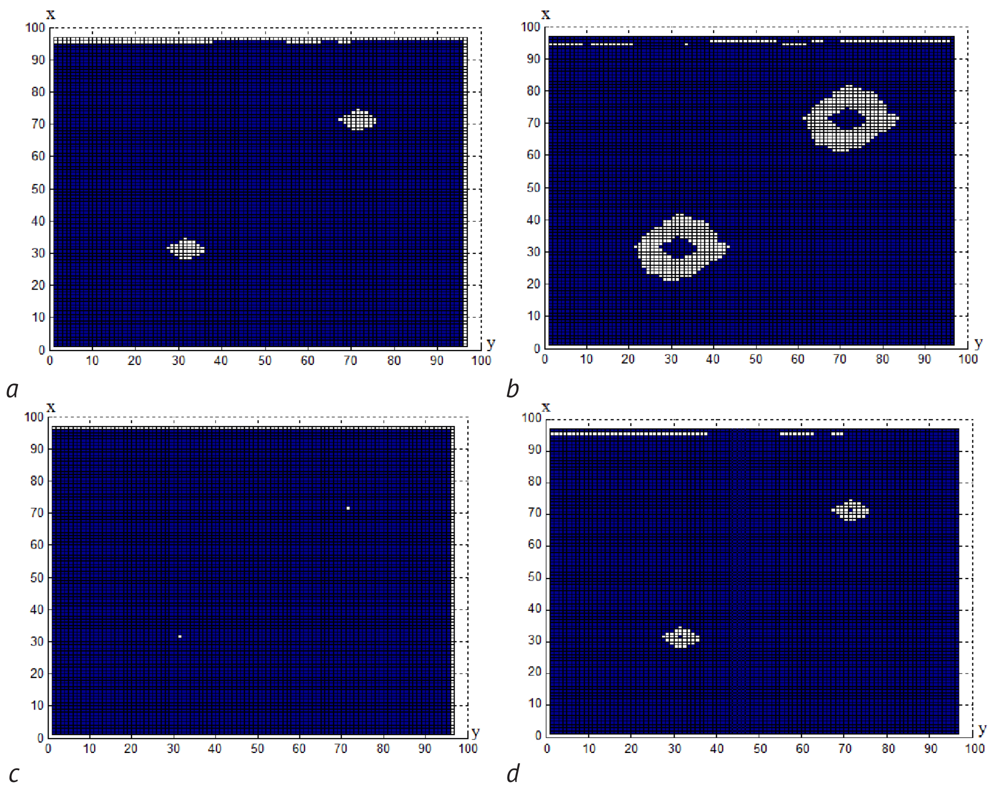

Figure 3. Sequence of sections for MAMBD DI subjected to cloning under conditions of additional disturbances
Notes: a -$1{,}094 \leq z \leq 2{,}700$; b – $2{,}701 \leq z \leq 4{,}307$; c – $1{,}094 \leq z \leq 1{,}897$; d – $1{,}898 \leq z \leq 2{,}700$
Source: created by the authors

In accordance with step 3 of the proposed method, the section $1{,}094 \leq z \leq 2{,}700$ is selected for further analysis (Fig. 3). Next, the segment [1,094, 2,700] is again divided in half, after which two more "sections" are constructed (Fig. 3). According to the criteria of the method, the interval $1{,}094 \leq z \leq 1{,}897$ is selected for further consideration. At this stage, the iterative analysis process is completed, since the area of identical objects in the corresponding binary image is equal to 1, i.e., the objects are point objects. As a result, given that $k_1 = k_2 = 1$, it is concluded that cloning is present in the analysed DI. In addition, the spatial location of the clone and its prototype is determined by isolated point objects, namely blocks with coordinates (31, 31) and (71, 71), which fully corresponds to the actual nature of the falsification (Fig. 3). Considering the original DI (Fig. 2), using the same parameter values for analysis as in the case of the falsified image (although in general this condition is not mandatory). Figure 4 shows the "sections" in the form of binary images obtained as a result of the first division of the interval $[a, b] = [T_{min}, T_{max}]$ in half.

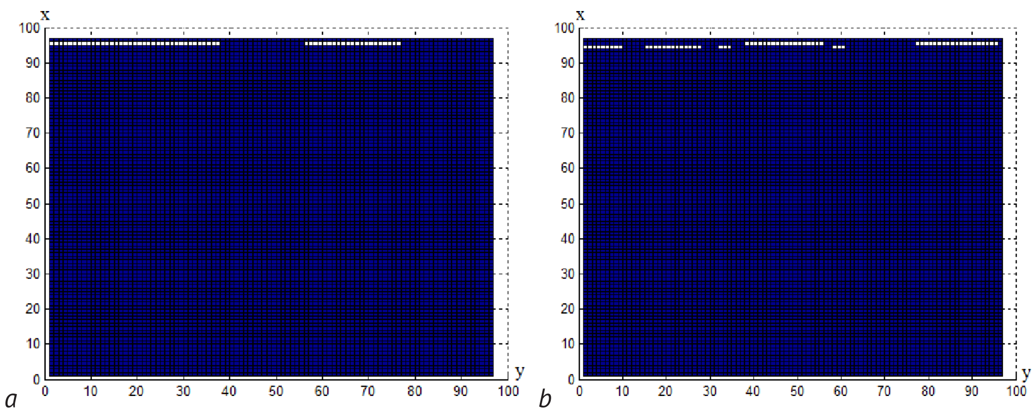

Figure 4. Sequence of cross-sections for the original DI
Notes: a -$1{,}094 \leq z \leq 2{,}700$; b – $2701 \leq z \leq 4{,}307$
Source: created by the authors

Further iterative refinement of the segment did not lead to qualitative changes in the form of the obtained sections, therefore the corresponding images are not shown. Analysis of the constructed binary images showed that no identical objects bounded by closed curves were found within any of the "sections". Accordingly, at this stage, the value $k_1 = k_2 = 0$ is recorded. At step 4 of the algorithm, based on the results obtained, a conclusion is made about the absence of cloning in the analysed DI, which is fully consistent with its actual status as original. The proposed MAMBD method of analysing the minimum block difference matrix does not in all cases provide an unambiguous clarification of the presence and spatial location of the clone and its prototype. The complexity of obtaining the result is due to the fact that the neighbourhoods of the clone and the prototype on the corresponding "sections" may not form closed curves in general. Moreover, in certain situations, such regions may represent discrete sets of points or short segments, which complicates their automated selection using standard DI processing methods.

As a result, the effectiveness of the MAMBD method is reduced for images with a weakly expressed structure or a high level of textural homogeneity, which requires the use of additional analysis criteria or combining the method with other approaches to detecting cloning results. Possible ways to overcome these limitations include combining the MAMBD method with additional criteria for spatial-structural analysis and using multi-level approaches to interpret the results. In particular, it is advisable to use morphological operations (expansion, narrowing, closing) to aggregate discrete points and segments into more connected areas, which facilitates their further selection and analysis. In addition, the stability of the localisation of the clone and prototype areas can be improved by adaptively changing the size of the analysed block q and using multi-scale analysis, which allows different levels of spatial detail in the image to be taken into account. Another promising direction is the integration of statistical and machine classification methods, in particular the use of clustering to group elements of the minimum block difference matrix that are close in value, or the use of machine learning models to distinguish between true and false positive manifestations of cloning. Additionally, the effectiveness of the method can be increased by combining MAMBD with feature-based approaches (based on key points, texture or frequency characteristics), which allows compensating for the shortcomings of each individual method and ensuring more reliable detection of cloning results in complex conditions of DI post-processing.

The results obtained confirm that the reliability of visual perception of DI and the stability of digital examination procedures significantly depend on the type and intensity of disturbing influences, as well as on their combinations. The paper justifies the use of PSNR as a quantitative criterion for controlling the "visual authenticity" of DI (threshold PSNR > 37 dB) and experimentally determines the ranges of noise, JPEG compression and filtering parameters at which distortions remain inconspicuous to humans, but can complicate or mask traces of forgery. This approach is consistent with the general trend in contemporary research in digital forensics in the work of W. Haiwei *et al.* (2022), which identifies not only the fact of manipulation, but also the robustness of methods to post-processing (noise, compression, filtering), which is a typical "anti-forensic" context. In the works of F.Z. Mehrjardi *et al.* (2023) and L.-X. Jiao *et al.* (2025), a significant part of the focus is on deep learning for detecting forgeries, in particular copy-move (cloning) and related manipulations, systematise deep learning approaches (CNN/transformer architectures, hybrids with "classical" features) and emphasise that the main challenge is degradation from real distribution channels (social networks, re-saving, filtering), which change image statistics and reduce the accuracy of detectors. The authors of the paper support the conclusions of these reviews: post-processing is a critical factor, and without an explicit "disturbance model" or at least quantitative quality control (such as PSNR), it is difficult to guarantee the reliability of expert conclusions.

At the same time, the recommended methodology differs from the dominant deep learning solutions in that it is interpretable and training-independent. The authors use an iterative procedure of dividing the interval $[T_{min}, T_{max}]$ in half and analysing the "sections" of the interpolated surface of the G matrix in the form of binary images. The decision on the choice of a subinterval is made based on the presence in both "sections" of objects of the same shape/size and their geometric characteristics (counters k_1, k_2), which allows localising the clone and prototype to point objects (area = 1) and determine the coordinates of the source blocks of the forgery. In practice, this brings our approach closer to a class of detectors that rely on stable structural/geometric manifestations of duplication characteristic of classical forensics (key points, block features), but implement localisation through controlled narrowing of the z parameter range rather than through mass comparison of descriptors. This complements the research of N.A.M. Abir *et al.* (2021), G. Suresh & C.S. Rao (2022), L.-X. Jiao *et al.* (2025), which describe keypoint-based and block-based CMFD methods.

The experimental conclusions of the authors of the work regarding the influence of JPEG compression, noise and filtering are consistent with the works of L. Bertojo *et al.* (2022), M. Aloraini *et al.* (2021), G. Tahaoglu *et al.* (2021), which demonstrate the robustness of CMFD to typical attacks (JPEG, Gaussian noise) under certain conditions, but also emphasise the dependence of the results on the intensity of degradation. In fact, Tables 1 – 4 in the paper show that the "acceptable" disturbance parameters (according to the PSNR criterion) are sharply narrowed under complex influences (noise + JPEG), which logically coincides with practical scenarios of online content distribution: consecutive re-encodings and platform-specific transformations can accumulate distortions. A similar emphasis on degradation from online environments is presented in the work of W. Haiwei *et al*. (2022), which proposes modelling "social media noise" and training robust detectors. Authors introduced a quantitative framework (PSNR threshold) for selecting disturbance modes under which visual authenticity is preserved but the forensic task is complicated. According to the reaserchers, this approach is useful both for evaluating the robustness of algorithms and for standardising experiments.

N. Taneja *et al*. (2025), C. Shi *et al*. (2023), H. Xie *et al*. (2022) emphasise that contrast enhancement, median filtering, or other transformations can be deliberately applied to mask traces of manipulation, and therefore detection methods must either be resistant to them or have quality control/change procedures in place. Observations by aforementioned authors on the significant impact of filtering (especially averaging with large windows) on PSNR and, accordingly, on "perceptual reliability" and potential detectability of cloning, and that filtering can "smooth out" local structures, which is critical for methods that rely on geometry/texture. J. Yang *et al*. (2021) proposed an algorithm based on key points or two-stage feature matching schemes and confirm that realistic attacks (scaling, rotations, noise, JPEG) are effective. The authors of the work emphasise that the difference between this approach and others is that instead of searching for a large number of matches, use iterative "sections" analysis and the criterion of minimising the geometric dimensions of objects as a convergence marker, which allows us to localise the clone/prototype in block coordinates and work in conditions of additional distortions controlled by PSNR. In summary, this work confirms the general conclusions of the current literature regarding the decisive role of post-processing and degradation in digital forensics tasks, but offers a more interpretable and parametrically controlled approach: the selection of acceptable perturbations through the PSNR threshold and the localisation of cloning through iterative interval division and analysis of binary "sections". At the same time, the practical value lies in the fact that this approach can be used as a standalone detection procedure or as a robustness assessment module/protocol for other CMFD methods (including deep learning) that have been actively developing in recent years.

CONCLUSIONS

As a result of the study, an urgent scientific and applied problem related to the development of a basic method for detecting cloning results in DI under the influence of additional disturbing factors has been solved. The proposed approach was based on the analysis of the minimum block difference matrix and the application of the segment splitting method, which provides a formalised procedure for detecting and localising the areas of the clone and its prototype. The paper justified the choice of types and parameters of disturbing influences that are most likely from a practical point of view and do not violate the reliability of visual perception of digital images. Based on computational experiments, quantitative threshold values for differences between corresponding clone and prototype blocks for different block sizes have been determined, which creates the basis for further algorithmic implementation of the method. It has been shown that the proposed algorithm allows not only to establish the fact of cloning, but also to determine the spatial location of the corresponding areas, while maintaining resistance to noise, filtering and lossy compression.

Further research should be directed towards improving the proposed method by integrating additional spatial-structural analysis criteria and morphological operations that allow discrete manifestations of cloning to be aggregated into connected regions. The development of a multi-scale approach with adaptive selection of the size of the analysed blocks depending on the local properties of the image, as well as the combination of MAMBD with feature-based, statistical and machine learning methods of analysis in order to reduce the number of false positive decisions, is promising. Of particular interest is the expansion of the class of studied disruptive influences, including complex combined attacks and geometric transformations, as well as the practical testing of the method in the tasks of digital forensics and information security. The implementation of these directions will increase the versatility, robustness and applied value of the proposed approach and create the prerequisites for the development of intelligent systems for the automated detection of DI falsification.

ACKNOWLEDGEMENTS

None.

FUNDING

None.

CONFLICT OF INTEREST

None.

REFERENCES

[1] Abir, N.A.M., Abd Warif, N. B., & Zainal, N. (2021) An evaluationofpatch match-based copy-move forgery detection (CMFD) onsocialmedia images. In *2021 IEEE international conference on artificial intelligence in engineering and technology (IICAIET)* (pp. 1-6). Kota Kinabalu: IEEE. doi: 10.1109/IICAIET51634.2021.9573571.

[2] Akram, A., Arfan, M., Rashid, J., Mahmood, K., & Ghani, A. (2025) Advanced digital image forensics: A hybrid framework for copy-move forgery detection in multimedia security. *Journal of Forensic Sciences*, 70 (5), 1801-1823. doi: 10.1111/1556-4029.70076.

[3] Ali, S.S., Ganapathi, I.I., Vu, N.-S., Ali, S.D., Saxena, N., & Werghi, N. (2022) Image forgery detection using deep learning by recompressing images. *Electronics*, 11(3), article number 403. doi: 10.3390/electronics11030403.

[4] Aloraini, M., Sharifzadeh, M., & Schonfeld, D. (2021) Sequential and patch analyses for object removal video forgery detection and localization. *IEEE Transactions on Circuits and Systems for Video Technology*, 31(3), 917-930. doi: 10.1109/tcsvt.2020.2993004.

[5] Bertojo, L., Néraud, C., & Puech, W. (2022) A very fast copy-move forgery detection method for 4K ultra HD images. *Frontiers in Signal Processing*, 2, article number 906304. doi: 10.3389/frsip.2022.906304.

[6] Duszejko, P., Walczyna, T., & Piotrowski, Z, (2025) Detection of manipulations in digital images: A review of passive and active methods utilizing deep learning. *Applied Sciences*, 15(2), 881. doi: 10.3390/app15020881.

[7] Gani, G., & Qadir, F. (2020) A robust copy-move forgery detection technique based on discrete cosine transform and cellular automata. *Journal of Information Security and Applications*, 54, article number 102510. doi: 10.1016/j.jisa.2020.102510.

[8] Ghai, A., Kumar, P., & Gupta, S. (2024) A deep-learning-based image forgery detection framework for controlling the spread of misinformation. *Information Technology & People*, 37(2), 966-997. doi: 10.1108/ITP-10-2020-0699.

[9] Grygorenko, S.N. (2016) Development of a method for detecting cloning in digital images under conditions of additional disruptive actions. *Legal, Regulatory and Metrological Support for the Information Protection System in Ukraine*, 1(31), 85-98.

[10] Haiwei, W., Zhou, J., Tian, J., & Liu, J. (2022) Robust image forgery detection over online social network shared images. In *IEEE/CVF conference on computer vision and pattern recognition (CVPR)* (pp. 13430-13439). New Orleans: IEEE. doi: 10.1109/CVPR52688.2022.01308.

[11] Hamza, A. (2022) *How to make salt pepper noise own code*. Retrieved from https://surl.li/empafc.

[12] Hosny, K.M., Mortda, A.M., Lashin, N.A., & Fouda, M.M. (2023) A new method to detect splicing image forgery using convolutional neural network. *Applied Sciences*, 13(3), article number 1272. doi: 10.3390/app13031272.

[13] Jain, A. (2024) *Salt and pepper noise and how to remove it in machine learning*. Retrieved from https://surl.lu/nezlap.

[14] Jaiswal, A.K., & Srivastava, R. (2022) Detection of copy-move forgery in digital image using multi-scale, multi-stage deep learning model. *Neural Processing Letters*, 54(1), 75-100. doi: 10.1007/s11063-021-10620-9.

[15] Jiao, L.-X., Ng, K.-W. & Tong, H.-L. (2025) A comprehensive review of keypoint-based copy-move forgery detection: Challenges and advances. *IEEE Access*, 13, 180941-180952. doi: 10.1109/ACCESS.2025.3618716.

[16] Kadam, K.D., Ahirrao, S., & Kotecha, K. (2022) Efficient approach towards detection and identification of copy move and image splicing forgeries using mask R-CNN with mobilenet V1. *Computational Intelligence and Neuroscience*, 1, article number 6845326. doi: 10.1155/2022/6845326.

[17] Khalil, A.H., Ghalwash, A.Z., Elsayed, H.A., Salama, G.I. & Ghalwash, H.A. (2023) Enhancing digital image forgery detection using transfer learning. *IEEE Access*, 11, 91583-91594. doi: 10.1109/ACCESS.2023.3307357.

[18] Koul, S., Kumar, M., Khurana, S.S., Mushtaq, F. ,& Kumar, K. (2022) An efficient approach for copy-move image forgery detection using convolution neural network. *Multimedia Tools and Applications*, 81(8), 11259-11277. doi: 10.1007/s11042-022-11974-5.

[19] Kundu, R. (2022) *Image processing: Techniques, types & applications*. Retrieved from https://www.v7labs.com/blog/image-processing-guide.

[20] Li, F., Pei, Z., Wei, W., Li, J., & Qin, C. (2022) Image forgery detection using tamper-guided dual self-attention network with multiresolution hybrid feature. *Security and Communication Networks*, 1, article number 1090307. doi: 10.1155/2022/1090307.

[21] Lumenci. (2024) *Digital image processing (DIP): A beginner's guide*. Retrieved from https://surli.cc/qwhewc.

[22] Mehrjardi, F.Z., Latif, A.M., Zarchi, M.S., & Sheikhpour, R. (2023) A survey on deep learning-based image forgery detection. *Pattern Recognition*, 144, article number 109778. doi: 10.1016/j.patcog.2023.109778.

[23] Shehin, A.U., & Sankar, D. (2024) Copy move forgery detection and localisation robust to rotation using block based discrete cosine transform and eigenvalues. *Journal of Visual Communication and Image Representation*, 99, article number 104075. doi: 10.1016/j.jvcir.2024.104075.

[24] Shi, C., Chen, L., Wang, C., Zhou, X., & Qin, Z. (2023). Review of image forensic techniques based on deep learning. *Mathematics*, 11(14), article number 3134. doi: 10.3390/math11143134.

[25] Suresh, G., & Rao, C.S. (2022) Detection and localization of copy-moveforgery in digital images: Review and challenges. *International Journal of Image and Graphics*, 23(4), article numer 2350025. doi: 10.1142/S0219467823500250.

[26] Tahaoglu, G., Uluas, G., & Ustubioglu, B. (2021) A new approach for localization of copy-move forgery in digital images. In *44th international conference on telecommunications and signal processing (TSP)* (pp. 183-186). Brno: IEEE. doi: 10.1109/TSP52935.2021.9522680.
[27] Taneja, M.E.N., Mishra, G.S., & Bhardwaj, D. (2025) Unmasking anti-forensic techniques: A DCNN-driven approach to uncover contrast enhancement and median filtering detection. *Journal of Forensic Sciences*, 70(6), 2324-2337. doi: 10.1111/1556-4029.70161.
[28] Xie, H., Ni, J., & Shi, Y.Q. (2022). Dual-domain generative adversarial network for digital image operation anti-forensics. *IEEE Transactions on Circuits and Systems for Video Technology*, 32(3), 1701-1706. doi: 10.1109/TCSVT.2021.3068294.
[29] Yang, J., Liang, Z., Gan, Y., & Zhong, J. (2021). A novel copy-move forgery detection algorithm via two-stage filtering. *Digital Signal Processing*, 113, article number 103032. doi: 10.1016/j.dsp.2021.103032.

Метод виявлення результатів клонування цифрових зображень в умовах постобробки

Світлана Григоренко

Кандидат технічних наук
Національний університет «Одеська політехніка»
65044, пр. Шевченка, 1, м. Одеса, Україна
https://orcid.org/0009-0006-4551-8243

Олександр Євсеєв

Старший викладач
Національний університет «Одеська політехніка»
65044, пр. Шевченка, 1, м. Одеса, Україна
https://orcid.org/0009-0009-3100-2643

Микола Воронов

Аспірант
Національний університет «Одеська політехніка»
65044, пр. Шевченка, 1, м. Одеса, Україна
https://orcid.org/0009-0003-2816-0495

Анотація. Актуальність цього дослідження обумовлена зростанням кількості випадків фальсифікації цифрових зображень та поширеним використанням клонування фрагментів як поширеної техніки маніпуляції, що створює серйозні виклики для інформаційної безпеки. Метою цього дослідження було розроблення та експериментальне підтвердження надійного методу виявлення клонування цифрових зображень в умовах постобробки на основі аналізу матриці мінімальної середньої різниці блоків, що дозволяє надійно ідентифікувати та просторово локалізувати клоновані області та їхні оригінальні прототипи. Запропонований метод базувався на ітеративному бісекційному інтервалі в поєднанні з бінарним перехресним аналізом різниць блоків і був реалізований в середовищі Matlab. Експериментальна структура включала моделювання адитивного гаусового, мультиплікативного та імпульсного шуму, стиснення JPEG, просторове фільтрування та комбіновані спотворення. Візуальна точність була кількісно оцінена за допомогою пікового відношення сигнал/шум із пороговим значенням відношення сигналу до шуму > 37 дБ. Обчислювальні експерименти проводилися на центральних областях цифрових зображень з роздільною здатністю 512×512 пікселів. Клоновані області займали менше 0,85 % площі зображення, зазвичай від 0,098 % до 0,39 %, при цьому також враховувалися менші клоновані області, менше 0,098 %. Аналіз проводився на випадково обраному одноколірному каналі з використанням блокової обробки. За відсутності спотворень після обробки глобальний мінімум функції мінімальної середньої різниці блоків досягав нуля, що забезпечувало максимальну ефективність виявлення з істинною позитивною частотою 100 %. Оцінка рівня помилкових позитивних результатів на оригінальних зображеннях дала значення 11 %, 7,5 % і 3 % для розмірів блоків 16, 24 і 32 відповідно. Рекомендований підхід демонструє високу чутливість виявлення, результати вказують на обмеження в придушенні помилкових позитивних результатів у порівнянні з деякими найсучаснішими методами, що підкреслює необхідність подальшої оптимізації

Ключові слова: пікове співвідношення сигналу до шуму; «сіль і перець»; гаусівський шум; мультиплікативний шум; «перетин»; Matlab